Environmental Science Nano

Mitochondria-targeted nanocarrier doubled the toxicity of oxidative phosphorylation and ATP synthesis disruptive insecticides against Spodoptera frugiperda

Journal:	*Environmental Science: Nano*
Manuscript ID	EN-ART-05-2022-000502.R2
Article Type:	Paper

Environmental Significance Statement

Pesticides play huge role in crop protection. However, the extensive use of pesticide is causing pressure on the environment and the unexpected side effects in non-target species. The development of functionalized nanocarriers which can improve the bioactivity of pesticides and decrease the pesticide application, showing great significance to ecological environment protection. Moreover, mesoporous silicates are environmentally friendly nanomaterials, which have great potential applications in nanomedicine and nano-pesticide.

Mitochondria-targeted nanocarrier doubled the toxicity of oxidative phosphorylation and ATP synthesis disruptive insecticides against *Spodoptera frugiperda*

Youwu Hao[a#], Di Liu[a#], Yonghui Song[a], Xinming Yin[a], Jia Liu[a*], Risong Na[a*] and Qing X. Li[b]

[a]National Key Laboratory of Wheat and Maize Crop Science, College of Plant Protection, Henan Agricultural University, 450002, Zhengzhou, China

[b]Department of Molecular Biosciences and Bioengineering, University of Hawaii at Manoa, 1955 East-West Road, Honolulu, HI 96822, USA

[#]These authors contributed equally to this work.

* Corresponding authors. Tel.: +86-371-63558170; fax: +86-371-63558170.

E-mail addresses: nrs@henau.edu.cn (R. Na) and ljia198346@163.com (J. Liu).

Abstract

Translocation and delivery of pesticides onto the molecular target is often a limiting step of efficacy, causing excessive use of pesticides and adverse effects on the environment and human health. Advances of nanomaterials have opened up a new avenue for effective translocation and delivery to increase the pesticide efficacy and reduce risks. We successfully synthesized and fully characterized a mesoporous silica nanoparticle-based mitochondria-targeted pesticide nanocarrier for the oxidative phosphorylation and ATP synthesis disruptor chlorfenapyr (Chl). The nanocarriers can be readily absorbed via oral and translocated into midgut and Malpighian duct of *Spodoptera frugiperda* larvae, and target mitochondria at the subcellular level. The Chl load content on the nanocarrier was up to 35%. The toxicity of the Chl-nanocarriers to the 3rd instar *S. frugiperda* (half maximum lethal concentration (LC_{50}), 16.4 μg/g expressed by the Chl content) was almost doubled relative to Chl alone (LC_{50} = 30.1 μg/g). Further research showed that the mitochondria-targeted nanocarrier enhanced Chl's efficacy by inducing mitochondrial damage in Sf9 cells, which led to the collapse of mitochondrial membrane potential and reduction of ATP production. The mitochondria-targeted nanocarriers have great application potential in formulation of oxidative phosphorylation and ATP synthesis disruptors, which can minimize their potential threats to food/environmental safety.

Keywords: Mesoporous silica nanoparticle; nanocarrier; mitochondria; chlorfenapyr; insecticide; formulation

1 Introduction

Insecticides are essential for protecting crops[1] from damages caused by pest insects such as *Spodoptera frugiperda* insects[2]. *S. frugiperda* is a destructive crop pest worldwide[3, 4] and attacks more than 350 plant species including various crops[5]. In sub-Saharan Africa alone, it threatens an annual crop loss of over $2.4–6.2 billion. Large quantities of insecticides, such as chlorantraniliprole[6], chlorpyrifos and lambda-cyhalothrin[7], are applied to control *S. frugiperda*, which can cause harms to humans and other non-targeted organisms. Undesirable effects of pesticides on the environment and ecosystems necessitate to increase the efficacy and reduce the use volume[8, 9]. Developing targeted delivery nanocarriers based on pesticide action mechanisms is a viable strategy. Therefore, it is necessary to introduce functional new formulation materials carrying pesticides to specific targets for efficacious pest control.

Chlorfenapyr (Chl) is a pro-insecticide used to control pest insects and mites on a variety of crops[10-12]. It has no cross-resistance to other classes of insecticides and is used in a number of countries[13]. Chl disrupts steps in the bioconversion pathway of adenosine tri-phosphate (ATP) from adenosine di-phosphate (ADP) in mitochondria[14], thus causes energy loss and subsequent death of the organism[14]. In China, Chl has been recommended for the control of the global pest *S. frugiperda*. Chl is also recommended by World Health Organization(WHO) for public health use[15]. As a result, the use of Chl has gradually increased, and it is one of Badische Anilin-und-Soda-Fabrik's (BASF) top five pesticides. In South Korea, the consumption of Chl was increased from 5,539 t in 2006 to 15, 821 t in 2014[16]. However, Chl can cause health issues[17-19]. For example,

chronic exposure of Chl can cause oxidative damage, apoptosis, and immune disorders in zebrafish liver[13, 20]. Moreover, cases of dog deaths due to acute Chl toxicity have been reported[21]. Some researchers have developed functional nanocarriers for Chl to improve its efficiency[20, 22]. Smart nanocarrier formulation, which releases Chl in mitochondria, can increase the efficacy of Chl for better *S. frugiperda* control and reduce undesired side effects[23].

Mesoporous silicates are nanomaterials, which have great potential applications in nanomedicine and nano-pesticide[9, 24, 25], and silica is abundant in the environment. Mesoporous silica nanoparticles (MSNs) may be among best pesticide carrier candidates in adhesion, immobilization and pesticide delivery[26, 27], due to the characteristic textural and structural features. The high surface area (1400 m^2/g), large pore volume (1-3 cm^3/g), very narrow distribution of pore size and open pore structures allow to load plenty of pesticides[28, 29]. Moreover, the external surface of MSNs is covered with silanol groups, which can be easily functionalized with organic functional groups, e.g., peptides[30] or polysaccharides[31] that can be recognized by receptors in tumor cells[32]. Generally, the biocompatibility, biodistribution, circulation time, cellular uptake, and drug efficacy of MSNs can all be affected by external functional modifications[31, 33]. In recent years, with the continuous advancement of research, MSNs modified with biocompatible and biodegradable compounds have been considered for formulating environmentally friendly agrochemicals[34-36]. Current research is mainly focused on the pesticide delivery system with special functions, such as pH responsive release[34]. Polymers for the functional modification of MSNs surface can be supplied by

triphenylphosphine (TPP), which is a kind of delocalized lipophilic cations. It can modify the surface of MSNs to form a mitochondria-targeting drug delivery carrier[37]. The carrier can be loaded with pesticides targeting mitochondria to achieve accurate release at the target, enhance the efficacy and reduce the application volume of pesticides.

In this study, we developed a mitochondria-targeting pesticide delivery nanocarrier based on MSNs for Chl. Chl-loaded mitochondria-targeting nanocarrier can be absorbed into S. frugiperda larvae via oral, and exhibits targeting function at cellular levels. Meanwhile, the ability and potential mechanism of nanocarrier to enhance Chl's efficacy on *S. frugiperda* control were studied, that is, it can enhance the activity of Chl by increasing mitochondrial damage. Targeted release of pesticides with functional carriers is an efficient way to improve the effect and reduce the amount of pesticide. The research of pesticide carriers using environmentally friendly materials is of great importance to utilization efficiency of agrochemicals and to environmental safety.

2 Materials and methods

2.1 Chemicals

Tetraethyl orthosilicate (TEOS, >99%), (3-aminopropyl) triethoxysilane (APTES, 99%), *N*-hydroxysuccinimide (NHS, 98%), and *N*-(3-dimethylaminopropyl)-*N*'-ethylcarbodiimide hydrochloride (EDC, 98.5%) were obtained from Macklin Ltd. (Shanghai, China). Cetyltrimethylammonium bromide (CTAB, >99%) was obtained from China National Pharmaceutical Group Corporation. Carboxymethyl chitosan (CMC) was obtained by Beijing HWRK Chem Co. Ltd. (Beijing, China). 4-

(Carboxybutyl) triphenylphosphonium bromide (CTPB, 98%) and fluorescein isothiocyanate (FITC, 95%) were obtained from J&K Scientific Ltd. (Beijing, China). Mito-Tracker red, ATP assay kit and mitochondrial membrane potential assay kit with rhodamine 123 were obtained from Beyotime (Shanghai, China). Chl was obtained from Sigma (St. Louis, MO, USA). Deionized water (DI water) was obtained from a Milli-Q water purification system from Millipore, USA. SFX-insect cell culture medium, fetal bovine serum (FBS), penicillin; and streptomycin were obtained from Thermo Fisher Scientific Inc. (Grand Island, NY, USA).

2.2 Cell culture

Solution of 1% streptomycin and penicillin (Hyclone) and 10% FBS (Gibco, USA) were added to SFX-insect cell culture medium. The prepared medium was used to culture *S. frugiperda* (Sf9) cells. The cells were incubated at 28 °C in an incubator. Fresh medium was used to replace the previous medium every 2 or 3 days.

2.3 Insects

S. frugiperda larvae were obtained from the Insect Bioassay Laboratory of Henan Agricultural University, China. They were reared in captivity in a chamber with a light phase of 12L:12D, 70 (±5) % relative humidity and 25 (±1) °C [38].

2.4 Synthesis of modified MSNs

2.4.1 Synthesis of MSNs

According to the sol-gel method[39], MSNs were synthesized with CTAB (template) and TEOS (silicon source). That is, CTAB (1g) was dissolved in DI water (480 mL) at 25°C, and sodium hydroxide solution (3.5 mL, 2 M) was added. After heating the

mixture to 80°C in an oil bath, TEOS (5.0 mL) was added dropwise. The mixture was vigorously stirred at 80 °C (6 h) and the resulting white precipitate was collected by vacuum filtration, dried in an oven at 80 °C (24 h) after washed three times with ethanol and water. Finally, the synthesized white powder was calcined at 550 ℃ for 5 h to obtain MSNs.

2.4.2 Synthesis of CMCs-4-TPP

CTPB (1.0 mmol, 0.443 g), NHS (1.5 mmol, 0.173 g) and EDC (1.5 mmol, 0.2876 g) were dissolved in DI water for 12 h for the activation of carboxyl group in CTPB. CMCs (1.0 mmol, 0.4 g) was then added to the solution. The solution was stirred at room temperate for 24 h, in order to allow the amine coupling reaction occurred between the carboxyl group of TPP (-COOH) and the amido group of CMCs ($-NH_2$). A dialysis bag (500 Da) was used to remove untreated materials and byproducts in the resulting product, dialyzed for 48 h with pure water (5 L). Lyophilization yielded dried CMCs-4-TPP.

2.4.3 Synthesis of MSN-CMCs and MSN-CMCs-TPP

The outer surface of MSNs was functionalized by post-grafting of APTES in anhydrous toluene[40]. Pristine MSNs (1 g) was suspended in anhydrous toluene (80 mL) and vigorously stirred for 20 min, and then with the addition of APTES (0.2 mL). The reaction mixture was refluxed for 4 h under vigorous stirring. After centrifugation at 11000 g for 5 min, the resultant samples were collected and washed with 80% aqueous ethanol three times. Nanoparticles (MSNs-NH_2) were acquired and dried at 80 ℃ for 24 h.

MSNs-NH_2 aqueous solution (0.6 g, 10 mL) with CMCs (1.0 mmol 0.44 g) formed amide bonds through the coupling reaction of amine and carboxyl groups under the promotion of EDC (5 mmol 0.959 g) and NHS (5 mmol 0.575 g), and finally generated MSN-CMCs.

CMCs-TPP (0.2 g) was dissolved in DI water (20 mL), and then with the addition of NHS (5 mmol 0.575 g) and EDC (5 mmol 0.959 g) in order to activate the carboxyl group of CMCs-TPP. After stirring at room temperature for 12 h, the MSNs-NH_2 aqueous solution (0.6 g, 10 mL) was added, and then continuously stirred for 24 h to complete the coupling reaction. After centrifugation at 11000 g for 5 min, the resulting product was collected and washed with 80% aqueous ethanol three times. Nanoparticles (MSN-CMCs-TPP) were obtained and dried at 60 ℃ for 6 h.

2.4.4 FITC labelled nanoparticles

Nanoparticles (0.2 g) were dispersed in anhydrous ethanol (50 mL). FITC (5 mg) was added and stirred for 24 h at ambient temperature. When the reaction was completed, the reaction solution was centrifuged under 11000 g for 5 min, washed with 80% aqueous ethanol (v/v) three times, dried overnight in the oven at 50 ℃. The product was wrapped in aluminum foil and stored at room temperature to preserve FITC label.

2.4.5 Chl-loaded nanocarriers

The O/W emulsions of Chl and CMCs-TPP were prepared: CMCs-TPP (0.2 g) and Tween-80 (0.2 mL) were dispersed in DI water (40 mL) to obtain the aqueous phase; Chl (0.4 g) was dissolved in dichloromethane (10 mL) to acquire the oil phase; In the homogenizer, the oil phase was dripped into the aqueous phase via centrifugation at

8,000 rpm for 15 min to produce a stable O/W emulsion.

The carboxyl group of CMCs-TPP was activated due to the addition of NHS (5 mmol 0.575 g) and EDC (5 mmol 0.959 g) to the emulsion. After stirring at room temperature for 6 h, MSNs-NH_2 was added and then stirred for 24 h, so that the amino group of MSNs-NH_2 reacted fully with the carboxyl group of CMCs-TPP. The collected product was washed with 80% aqueous ethanol (v/v) three times. The obtained MSN-CMCs-TPP nanoparticles which loaded with Chl were dried at 60 ℃ for 6 h. MSN-CMCs nanoparticles loaded with Chl was synthesized by the same method.

2.5 Nanoparticle characterization

A Fourier transform infrared spectroscopy (FT-IR) instrument (Thermo Fisher Scientific, Waltham, Massachusetts, USA) was used to observe the chemical grafting processes occurring with the nanoparticles[41]. Nanoparticles were treated by potassium bromide pellets and measured at a resolution of 4 cm^{-1} in the spectral region between 4000 and 400 cm^{-1}.

Visualization of morphology and structure were performed by scanning electron microscope (SEM, SU8010, Hitachi, Ltd., Tokyo, Japan) and transmission electron microscopy (TEM, Tecnai G2, F20 S-TWIN, FEI, Oregon, USA) on the nanoparticles. The dried sample powder is carefully fixed on the conductive adhesive, then the sample is purged and sprayed with gold, dried in vacuum, and then analyzed by SEM. The sample powder was dispersed in an ethanol solution, dried in the air, a drop of the suspension containing the sample powder was adsorbed on the carbon-coated copper net, and then analyzed by TEM. The average particle size of nanoparticles can be

measured by statistical analysis of three SEM images.

In nitrogen environment, the thermogravimetric analysis was carried out by using a NETZSCH STA 449F3 (NETZSCH- Gerätebau GmbH, Germany) thermogravimetric/differential thermal analyzer (the heating rate is 15 ℃/min). Date was collected to analyze the stability of nanoparticles and the loading amount of functional modified groups in the range of 30-800 ℃.

Monitoring of N2 adsorption - desorption isotherms using a specific surface area and aperture analyzer (ASAP 2460, Micromeritics Instruments Corp, Norcross, GA, USA) under continuous adsorption conditions.

The aperture distribution and the specific surface areas can be estimated by using BET equation[42] and BJH method[43] respectively, and then the related properties of the nanoparticle carrier can be determined.

A Zetasizer Nano ZS analyzer (Microtrac, San Diego, CA, USA) with dynamic light scattering (DLS) was used to measure the Zeta potential and particle size of nanoparticles. Solution required for test (1 mg/mL) were prepared with water. Before determination, each solution was ultrasonic treated for 5 minutes to prevent any aggregation. Each sample was measured three times to achieve average value.

2.6 Calculation of loading content and encapsulation efficiency

The loading (%) and encapsulation efficiency (%) of Chl were calculated according to the following formulas: loading content (%) = (weight of Chl encapsulated in nanoparticles/weight of nanoparticles) × 100; encapsulation efficiency (%) = (weight of Chl encapsulated in nanoparticles/initial weight of Chl employed) × 100.

The MSN-CMCs-TPP-Chl (10 mg) were prepared and extracted with 50 mL ethanol for 4 hours at 25℃, then the solution was centrifuged at 8000 rpm for 4 min and washed with 100 mL ethanol for three times. The content of Chl in the washings was determined by high-performance liquid chromatography (HPLC, 1200 Series, Agilent, Santa Clara, CA, USA) using the following HPLC conditions: chromatographic column, C18 (5 μm × 4.6 mm × 250 mm, Agilent, Santa Clara, CA, USA); mobile phase, a mixture of acetonitrile and water (80:20, v/v); flow rate, 1.0 mL/min; injection volume, 5 μL; and 245 nm wavelength detection.

2.7 In vivo fluorescence imaging

A solution of test ingredient in methanol was added to the artificial diet: MSN-CMCs-TPP-FITC at final concentrations of 100 μg/g. The glass tubes (8.5 cm × 2.5 cm) were sterilized, loading feed and introducing the 3rd instar larvae of *Spodoptera frugiperda* into the glass tubes individually. After 24 h, the larvae were dissected to obtain the epidermis, midgut, and washed three times with PBS. The nanoparticle carrier in vivo was visualized by fluorescence microscopy (488 nm, ×25, ×100 Leica Microsystems, DMI 3000B, GER).

2.8 Colocalization of mitochondria and nanoparticles in Sf9 cells

Antibiotics (streptomycin and penicillin) were added to the SFX-insect cell culture medium at 1% and fetal bovine serum was added to the SFX-insect cell culture medium at 10%[44]. Prepared medium was used to cultivate *S. frugiperda* (Sf9) cell line (ATCC, CRL-1711). An incubator which maintained at 28°C was used to culture cells.

Mito-Tracker Red is a commercial mitochondrial red fluorescent probe with a wide

range of applications. This live cell probe enables mitochondria-specific fluorescent staining. FITC is a commercial probe with green fluorescence for localization of nanoparticles. The colocalization imaging experiment of mitochondrial and nanoparticle was achieved by the two probes. Sf9 cells were treated by MSN-CMC-FITC and MSN-CMCs-TPP-FITC (100 μg/mL) for 2 h, and hereafter incubated for 30 min with Mito-Tracker Red (0.5 μM). In the end, a Nikon confocal microscope (×100, Nikon, Melville, NY, USA) was used to photograph and analyze the counterstaining cells. Emission at 488 nm was collected for FITC and 561 nm for Mito-Tracker Red[45].

2.9 Biological activity

Thirty 30 3rd instar *S. frugiperda* larvae were used in each treatment and control. A solution of test ingredient in methanol was added to the artificial diet: Chl at final concentrations of 8.87, 17.73, 35.45 and 53.18 μg/g; MSN-CMCs-TPP at final concentrations of 25, 50, 100 and 150 μg/g; MSN-CMCs-TPP-Chl at final concentrations of 33.86, 67.73, 135.45 and 203.18 μg/g. The loading content (%) of Chl was 35.4% i.e., 135.45 g MSN-CMCs-TPP-Chl contained 100 g MSN-CMCs-TPP and 35.45 g Chl. Diet for the control was the same as that for the treatment except without CHl, MSN-CMCs-TPP and MSN-CMCs-TPP-Chl. Daily observations were made and dead insects were counted at the end of each phase, for five days.

2.10 ATP content assay

The determination of intracellular ATP Levels is according to the manufacturer instructions. Briefly, sf9 cells were treated with Chl (35.45 μg/mL), MSN-CMCs-TPP (100 μg/mL) and MSN-CMCs-TPP-Chl (135.45 μg/mL) for 2 h, followed by treatment

in lysis buffer at 4 °C for 30 min. Solution was centrifuged at 16000 g for 15 min, and part of the supernatant was transferred into a 96-well plate to determine the ATP activity.

2.11 Detection assay of mitochondrial membrane potential ($\Delta\Psi m$)

The measurement of mitochondria membrane polarization can be achieved by Rhodamine (Rh-123) fluorescence, that is due to the accumulation of Rh-123 in membranes by a membrane polarization dependent-manner way[46]. The detection of the mitochondrial transmembrane potential ($\Delta\Psi m$) loss was carried out by the fluorescence microscopy combining with Rh-123, in order to indicated the mitochondrial damage caused by Chl, MSN-CMCs-TPP and MSN-CMCs-TPP-Chl[47]. Sf9 cells were treated by Chl (35.45 μg/mL), MSN-CMCs-TPP (100 μg/mL) and MSN-CMCs-TPP-Chl (135.45 μg/mL) for 2 h. Cell photos are taken under a fluorescence microscope (488 nm, × 100), after the cells were stained by Rh-123.

2.12 Statistical analysis

Each experiment was carried out in triplicate. Data were analyzed with SPSS version 17.0, statistical program (SPSS Inc., Chicago, IL, USA). Data were the mean ± standard deviation (SD). The judgement of the differences with control in each experiments were subjected to one-way analysis of variance (ANOVA) with Dunnet's test (*, $P \leq 0.05$; **, $P \leq 0.01$)[48].

3 Results and Discussion

Chl targets mitochondria and disrupts the intracellular conversion of ADP to ATP, resulting in a loss of energy in insects, leads to cellular dysfunction and subsequent

death[14]. MSNs show significant advantages over traditional drug nanocarriers[49]. It is not only a mature low-cost nanomaterial, but also a soil-friendly nanomaterial. Therefore, MSN mitochondria-targeted nanocarriers was synthesized for Chl based on MSNs. In this study, in order to improve the efficacy of pesticides and reduce the use of pesticides, TPP-modified MSN was developed as a targeted delivery carrier for Chl. Its physicochemical properties, mitochondria targeting properties and the effect of improving the biological activity of Chl were investigated.

3.1 Modification and characterization of nanoparticles

The successful modification and pesticide loading of MSNs were revealed by FT-IR (Fig 1A) and Zeta potential assay (Fig 3C). The main infrared characteristic peaks of MSNs were Si-O-Si. The peak at 1072 cm^{-1} is the antisymmetric stretching vibration absorption peak of Si-O-Si bond. The peak near 1645 cm^{-1} is the antisymmetric stretching vibration characteristic peak of -C=O in CMC, which overlap the characteristic peak of $-NH_2$ in this region[34]. The characteristic peaks of -C=O of CMC on MSN-CMCs were also observed. The FT-IR spectra of the TPP-modified CMCs (CMCs-TPP) showed that the characteristic stretching absorption peak near the 1361 cm^{-1} of TPP in CMCs-TPP (Fig 1B). The FT-IR spectra of MSN-CMCs-TPP (Fig 1C) showed the characteristic absorption peaks of MSNs, CMC and TPP, indicating successful modification of MSNs by CMCs-TPP. The FT-IR spectra of MSN-CMCs-TPP-Chl (Fig 1D) showed the characteristic absorption peaks of Chl (1645 cm^{-1}), indicating successful loading of Chl on functional nanoparticle.

The initial Zeta potential of MSNs was -23.9 mV and the Zeta potential of MSNs-

NH_2 rose to 22.16 mV (Fig 3C and Table 1), due to the addition of positively charged-NH_2 on the surface of the carrier. However, the introduction of negatively charged CMCs-TPP and CMCs-TPP-Chl on the surface led to a sharp decrease in Zeta potential to -96.8 mV and -102.1 mV, respectively. All the results showed successful synthesis of MSN-CMCs-TPP and load of CH1 to the MSN-CMCs-TPP.

MSNs have significant advantages in application of agrochemicals because of their structural properties and environmental compatibility. The visualization of nanoparticles' morphology was achieved by SEM and TEM (Fig 2). As shown in Fig 2A, MSN, MSN-CMCs-TPP and MSN-CMCs-TPP-Chl were spherical nanoparticles. The surface of MSNs was relatively smooth, whereas the surface of MSNs modified by CMCs-TPP became rough (Fig 2B). The average particle size of nanoparticles was determined via statistical analyses of the SEM images of more than 100 nanoparticles. The surface modification slightly increased the average particle size of the nanoparticles from 123 nm (MSNs) to 145 nm (MSN-CMCs-TPP) and 237 nm (MSN-CMCs-TPP-Chl) (Table 1).

Thermal stability is another important indicator of nanocarriers. A thermogravimetric analysis (TGA) curve can be used to study the thermal stability and general decomposition behavior of carrier materials. Fig 3A shows that the weight loss of MSNs was almost zero and the weight loss of MSN-CMCs and MSN-CMCs-TPP were slightly in the temperature range between 250 ℃ and 700 ℃, which indicates that MSNs have loaded other groups and the functionalized nanocarriers have good thermal stability below 250 ℃. TGA also proved the successful loading of Chl on the

nanoparticles.

Under the condition of constant temperature provided by liquid nitrogen, the measurement and calculation of carrier materials' specific surface area and pore size were carried out by an automatic specific surface area and pore analyzer. The nitrogen adsorption and analytical isotherm were obtained with the BET equation. The MSNs isotherm belongs to type IV in the IUPAC classification (Fig 3B). The type IV adsorption isotherm is usually attributed to mesoporous adsorption behaviors. The type IV adsorption isotherm without hysteresis ring indicates that the mesoporous diameter of the nanoparticles was less than 4 nm. In the range of P/P0 = 0-0.2, nitrogen molecules undergo a single-layer to multi-layer adsorption process on the mesoporous wall of the material, while in the range of P/P0 = 0.2-0.4, it is caused by the liquefaction of nitrogen molecules in the pores. At P/P0 = 0.4-0.9, the adsorption of nitrogen molecules in the channel reached equilibrium, and when P/P0 > 0.9, the gap between the samples condensed liquid nitrogen, which led to the increase of nitrogen adsorption. Table 1 shows that the S_{BET} and Vt of MSNs were 1358 m^2/g and 1.23 cm^3/g, while the S_{BET} and Vt of CMCs-TPP-modified MSNs were significantly decreased to 45 m^2/g and 0.11 cm^3/g. That is because these groups have a significant sealing effect on the outer layer of MSNs, resulting in a decrease in internal specific surface area and total pore volume

The loading rate and encapsulation efficiency of the nanoparticles were obtained via HPLC analysis (Table 2). The functionally modified nanoparticles (i.e., MSN-CMCs-TPP) were less Chl-loaded as determined with the impregnation method. Combined with the characterization of the specific surface area of the carrier and Zeta

potential, the functional modified group (i.e., CMC) may wrap the nanoparticles too tightly, so that Chl can't be freely dispersed into the modified MSNs. This defect was obviously improved through the emulsion synchronous encapsulation technology (loading content *ca.* 34.4 %). Compared with the pesticide loading of simple MSNs, the functionalized MSNs can achieve almost the same entrapment efficiency as emulsion synchronous encapsulation technology. Therefore, when the functionalized nanoparticles are loaded with pesticides, the emulsion synchronous encapsulation method can give full play to the performance of MSN.

3.2 TPP confers mitochondria targeting properties in MSNs

The mitochondria targeting properties were evidenced by vivo uptake and further subcellular localization. As shown in Fig. 4, after *S. frugiperda* larvae being treated with MSN-CMCs-TPP-FITC for 24 h, the fluorescence of FITC was more abundant in midgut and Malpighian tubules than that in epidermis. Which indicating that Chl-nanocarriers can be readily absorbed via oral and translocated into midgut and Malpighian duct of *S. frugiperda* larvae. As shown in Fig. 5, after cells being treated with MSN-CMCs and MSN-CMCs-TPP for 4 h, comparing with MSN-CMCs group, the fluorescence from FITC in MSN-CMCs-TPP treated group displayed a significant increase. Furthermore, in the MSN-CMCs-TPP-treated group, the nanoparticles co-localized with mitochondria and showed yellow fluorescence, which indicating that the nanocarrier MSN-CMCs-TPP has the ability of mitochondria targeting.

3.3 Enhancement of Chl insecticidal activity by the nanoparticle carrier

In order to explore whether the mitochondria targeting nanocarrier can enhance

Chl's insecticidal activity, we determined insecticidal activity, mitochondrial membrane potential ($\Delta\Psi m$) and ATP content.

Mitochondria targeting nanocarrier MSN-CMCs-TPP enhanced mortality of Chl on larvae of *S. frugiperda* (Fig 6A). Chl and MSN-CMCs-TPP-Chl were toxic to *S. frugiperda* larvae, and the mortality of 3rd-instar larvae significantly increased 72 h after exposure. Chl at 53.2 μg/g showed over 80% mortality. The nanoparticle MSN-CMCs-TPP alone at a dose of 150 μg/g had less than 15% of the mortality 72 h after exposure. However, the toxicity of Chl on *S. frugiperda* larvae was significantly enhanced by use of mitochondria targeting nanocarrier MSN-CMCs-TPP. MSN-CMCs-TPP-Chl at 203 μg/g caused greater than 90% mortality of the 3rd-instar larvae (Fig.6A). Median lethal concentrations (LC_{50}) and toxicity regression equations of three treatments on the mortality of 3rd instar *s. frugiperda* were listed in Table 3. LC_{50} of Chl was 30.1 μg/g to *S. frugiperda* larvae. The nanoparticle MSN-CMCs-TPP alone showed no significantly toxicity 72 h after exposure. But the LC_{50} values of MSN-CMCs-TPP-Chl was 62.7 μg/g, which was 16.4 μg/g as expressed by the Chl equivalent. The data suggest that the nanocarrier can double the toxic effect of Chl on *S. frugiperda* larvae.

Mitochondria are essential for eukaryotic cells. MSN-CMCs-TPP enhanced Chl's ability to induce mitochondrial damage (e.g., collapse of mitochondrial membrane potential) and reduce ATP production in Sf9 cells. After the $\Delta\Psi m$ was dissipated, the cells entered an irreversible process of apoptosis. The changes of intracellular $\Delta\Psi m$ caused by Chl, MSN-CMCs-TPP and MSN-CMCs-TPP-CH1 were evidenced by the

fluorescence intensity changes of Rh-123 (Fig. 6B). The images displayed a decrease of fluorescence in Sf9 cells of Chl and MSN-CMCs-TPP-Chl treated groups, which illustrated depolarization of $\Delta\Psi m$. Meanwhile, the fluorescence intensity in MSN-CMCs-TPP-Chl treatment group was obviously less than Chl treatment groups, which indicated that with the use of mitochondria targeting nanocarrier, the reduction of $\Delta\Psi m$ in Sf9 cells caused by Chl was getting more seriously. Comparing with the control group, the reduction of cellular ATP in Chl and MSN-CMCs-TPP-CH1 treated Sf9 cells were evidenced, and the MSN-CMCs-TPP-Chl treated group decreased more than the CH1 treated group (Fig. 6C).

These results indicated that mitochondria targeting nanocarrier MSN-CMCs-TPP increase mortality of Chl on larvae of *S. frugiperda* by increasing the mitochondrial damage at the same concentration of Chl.

4 Conclusion

This study developed a drug delivery system (MSN-CMCs-TPP) with mitochondria-targeting function based on MSNs for the mitochondria-targeting insecticide Ch1. The obtained MSN-CMCs-TPP nanoparticle has the characteristics of mitochondria targeting, high loading (35.45%), and absorption. The mitochondria-targeted nanocarrier system (MSN-CMCs-TPP) enhanced the mortality of Chl to *S. frugiperda* lavae (LC_{50} decreased from 30.1 μg/g to 16.4 μg/g). MSN-CMCs-TPP contributes Chl's ability to damage mitochondria in Sf9 cells, being the probable mechanism of the improved insecticidal potency of Chl. This study demonstrated specific applications of the nanomaterials in agriculture. Functionalized nanocarriers

improve the bioactivity of synthetic pesticides and decrease the pesticide application, showing great potential for green pest management. The research is of high value to designing smart pesticide formulations and advanceing sustainable agriculture.

Authors' contributions - provide individual author contribution

Risong Na and Youwu Hao designed the experiments. Youwu Hao, Di Liu and Yonghui Song carried out the experiments, interpreted the results. Youwu Hao wrote the main manuscript text. Risong Na, Jia Liu, Xinming Yin and Qing X. Li revised the manuscript. All authors reviewed the manuscript.

Conflict of Interest Statement

The authors declare no conflict of interest.

Acknowledgements

This work was financially supported in part by the National Natural Science Foundation of China (NO.21702048 and NO. U1904111), Earmarked fund for China Agriculture Research System (NO. CARS-27), and the USDA (HAW05044-R).

References

1. M. R. Uddin, S. U. Park, F. E. Dayan and J. Y. Pyon, Herbicidal activity of formulated sorgoleone, a natural product of sorghum root exudate, *Pest. Manage. Sci.*, 2014, **70**, 252-257.
2. X. C. Morales, A. Tamiru, I. S. Sobhy, T. J. A. Bruce, C. A. O. Midega and Z. Khan, Evaluation of African Maize Cultivars for Resistance to Fall Armyworm Spodoptera frugiperda (J. E. Smith) (Lepidoptera: Noctuidae) Larvae, *Plants-Basel*, 2021, **10**.
3. L. Scheidegger, S. Niassy, C. Midega, X. Chiriboga, N. Delabays, F. Lefort, R. Zurcher, G. Hailu, Z. Khan and S. Subramanian, The role of Desmodium intortum, Brachiaria sp. and Phaseolus vulgaris in the management of fall armyworm Spodoptera frugiperda (J. E. Smith) in maize cropping systems in Africa, *Pest. Manage. Sci.*, 2021, **77**, 2350-2357.
4. E.-L. Zhan, Y. Wang, J. Jiang, Z.-Q. Jia, T. Tang, Z.-J. Song, Z.-J. Han and C.-Q. Zhao, Influence of three insecticides targeting GABA receptor on fall armyworm Spodoptera frugiperda: Analyses from individual, biochemical and molecular levels, *Pestic. Biochem. Physiol.*, 2021, **179**.
5. D. G. Montezano, A. Specht, D. R. Sosa-Gomez, V. F. Roque-Specht, J. C. Sousa-Silva, S. V. Paula-Moraes, J. A. Peterson and T. E. Hunt, Host plants of Spodoptera frugiperda (Lepidoptera: Noctuidae) in the Americas, *Afr. Entomol.*, 2018, **26**, 286-300.
6. D. Boaventura, A. Bolzan, F. E. O. Padovez, D. M. Okuma, C. Omoto and R. Nauen, Detection of a ryanodine receptor target-site mutation in diamide insecticide resistant

fall armyworm, Spodoptera frugiperda, *Pest. Manage. Sci.*, 2020, **76**, 47-54.

7. R. A. Carvalho, C. Omoto, L. M. Field, M. S. Williamson and C. Bass, Investigating the Molecular Mechanisms of Organophosphate and Pyrethroid Resistance in the Fall Armyworm Spodoptera frugiperda, *PLoS One*, 2013, **8**.

8. Y. Hao, Y. Zhang, W. Xu, J. Gao and L. Tao, Synergistic effects of adjuvant A-134 on the herbicidal effects of glyphosate, *Journal of Pesticide Science*, 2019, **44**, 249-254.

9. A. Popat, J. Liu, Q. Hu, M. Kennedy, B. Peters, G. Q. Lu and S. Z. Qiao, Adsorption and release of biocides with mesoporous silica nanoparticles, *Nanoscale*, 2012, **4**, 970-975.

10. F. H. Arthur, Dosage rate, temperature, and food source provisioning affect susceptibility of Tribolium castaneum and Tribolium confusum to chlorfenapyr, *Journal of Pest Science*, 2013, **86**, 507-513.

11. M. Ahmad and R. Mehmood, Monitoring of Resistance to New Chemistry Insecticides in Spodoptera litura (Lepidoptera: Noctuidae) in Pakistan, *J. Econ. Entomol.*, 2015, **108**, 1279-1288.

12. S. Ullah, R. M. Shah and S. A. Shad, Genetics, realized heritability and possible mechanism of chlorfenapyr resistance in Oxycarenus hyalinipennis (Lygaeidae: Hemiptera), *Pestic. Biochem. Physiol.*, 2016, **133**, 91-96.

13. X. Chen, J. Zheng, M. Teng, J. Zhang, L. Qian, M. Duan, F. Zhao, W. Zhao, Z. Wang and C. Wang, Bioaccumulation, Metabolism and the Toxic Effects of Chlorfenapyr in Zebrafish (Danio rerio), *J. Agric. Food. Chem.*, 2021, **69**, 8110-8119.

14. A. Younas, H. N. Rashid, D. Hussain, S. T. R. Naqvi, M. A. Khan, B. Fatima and S.

Majeed, Chlorfenapyr containing anions uptake from industrial wastewater by ethylene glycol functionalized benzyl dimethyl tetradecyl ammonium bromide membrane, *J. Environ. Manage.*, 2021, **284**.

15. J. Z. Yuan, Q. F. Li, J. B. Huang and J. F. Gao, Effect of chlorfenapyr on cypermethrin-resistant Culex pipiens pallens Coq mosquitoes, *Acta Trop.*, 2015, **143**, 13-17.

16. D.-K. Jeong, H.-J. Lee, J.-Y. Bae, Y.-S. Jang, S.-M. Hong and J.-H. Kim, Chlorfenapyr Residue in Sweet Persimmon from Farm to Table, *J. Food Prot.*, 2019, **82**, 810-814.

17. R. M. Oxborough, R. N'Guessan, R. Jones, J. Kitau, C. Ngufor, D. Malone, F. W. Mosha and M. W. Rowland, The activity of the pyrrole insecticide chlorfenapyr in mosquito bioassay: towards a more rational testing and screening of non-neurotoxic insecticides for malaria vector control, *Malar. J.*, 2015, **14**.

18. K. Dang, S. L. Doggett, G. V. Singham and C.-Y. Lee, Insecticide resistance and resistance mechanisms in bed bugs, Cimex spp. (Hemiptera: Cimicidae), *Parasites & Vectors*, 2017, **10**.

19. A. A. Romeh and R. A. I. Saber, Green nano-phytoremediation and solubility improving agents for the remediation of chlorfenapyr contaminated soil and water, *J. Environ. Manage.*, 2020, **260**.

20. L. Zhu, G. Jiang, J. Cen and L. Li, Preparation and performance of chlorfenapyr microcapsules with a degradable polylactide-based polyurethane wall material, *RSC Adv.*, 2022, **12**, 16918-16926.

21. R. B. Davy, S. Campos and A. M. Lynch, Acute chlorfenapyr toxicity in 3 dogs from a single household, *Journal of Veterinary Emergency and Critical Care*, 2019, **29**, 686-

689.

22. S. Yan, H. Yin, N. Li, Y. Chen, C. Ji, Q. Jiang, J. Du, M. Yin, J. Shen and J. Zhang, Combination of a nanocarrier delivery system with genetic manipulation further improves pesticide efficiency: a case study with chlorfenapyr, *Environmental Science-Nano*, 2022, **9**, 2020-2031.

23. P. Nittayacharn and N. Nasongkla, Development of self-forming doxorubicin-loaded polymeric depots as an injectable drug delivery system for liver cancer chemotherapy, *Journal of Materials Science-Materials in Medicine*, 2017, **28**.

24. N. Gomez-Cerezo, I. Izquierdo-Barba, D. Arcos and M. Vallet-Regi, Tailoring the biological response of mesoporous bioactive materials, *J. Mater. Chem. B*, 2015, **3**, 3810-3819.

25. Z. Qinghong, Y. Chang, C. Xuanli, W. Yue, B. Yulong, L. Chengyue, L. Haixiang, G. Zhimin, C. Tingwei, R. Zhijie, Q. Yao, Z. Yunhua, M. Kangsheng, L. Jianhong, H. Shun and W. Hu, CeO2 nanohybrid as a synergist for insecticide resistance management, *Chem. Eng. J. Adv.*, 2022, **446**, 137074.

26. R. R. Castillo, A. Baeza and M. Vallet-Regi, Recent applications of the combination of mesoporous silica nanoparticles with nucleic acids: development of bioresponsive devices, carriers and sensors, *Biomater. Sci.*, 2017, **5**, 353-377.

27. S. Rahmani, J.-O. Durand, C. Charnay, L. Lichon, M. Ferid, M. Garcia and M. Gary-Bobo, Synthesis of mesoporous silica nanoparticles and nanorods: Application to doxorubicin delivery, *Solid State Sci.*, 2017, **68**, 25-31.

28. J. L. Paris, M. V. Cabanas, M. Manzano and M. Vallet-Regi, Polymer-Grafted

Mesoporous Silica Nanoparticles as Ultrasound-Responsive Drug Carriers, *ACS Nano*, 2015, **9**, 11023-11033.

29. F. Sevimli and A. Yilmaz, Surface functionalization of SBA-15 particles for amoxicillin delivery, *Microporous Mesoporous Mater.*, 2012, **158**, 281-291.

30. Z.-Y. Li, J.-J. Hu, Q. Xu, S. Chen, H.-Z. Jia, Y.-X. Sun, R.-X. Zhuo and X.-Z. Zhang, A redox-responsive drug delivery system based on RGD containing peptide-capped mesoporous silica nanoparticles, *J. Mater. Chem. B*, 2015, **3**, 39-44.

31. A. Salis, M. Fanti, L. Medda, V. Nairi, F. Cugia, M. Piludu, V. Sogos and M. Monduzzi, Mesoporous Silica Nanoparticles Functionalized with Hyaluronic Acid and Chitosan Biopolymers. Effect of Functionalization on Cell Internalization, *ACS Biomater. Sci. Eng.*, 2016, **2**, 741-751.

32. M. Chang, F. Zhang, T. Wei, T. Zuo, Y. Guan, G. Lin and W. Shao, Smart linkers in polymer-drug conjugates for tumor-targeted delivery, *J. Drug Targeting*, 2016, **24**, 475-491.

33. L. Medda, M. F. Casula, M. Monduzzi and A. Salis, Adsorption of Lysozyme on Hyaluronic Acid Functionalized SBA-15 Mesoporous Silica: A Possible Bioadhesive Depot System, *Langmuir*, 2014, **30**, 12996-13004.

34. C. Xu, L. Cao, P. Zhao, Z. Zhou, C. Cao, F. Li and Q. Huang, Emulsion-based synchronous pesticide encapsulation and surface modification of mesoporous silica nanoparticles with carboxymethyl chitosan for controlled azoxystrobin release, *Chem. Eng. J.*, 2018, **348**, 244-254.

35. C. Xu, Y. Shan, M. Bilal, B. Xu, L. Cao and Q. Huang, Copper ions chelated

mesoporous silica nanoparticles via dopamine chemistry for controlled pesticide release regulated by coordination bonding, *Chem. Eng. J.*, 2020, **395**.

36. Y. Wang, S. Song, X. Chu, W. Feng, J. Li, X. Huang, N. Zhou and J. Shen, A new temperature-responsive controlled-release pesticide formulation - poly(N-isopropylacrylamide) modified graphene oxide as the nanocarrier for lambda-cyhalothrin delivery and their application in pesticide transportation, *Colloids and Surfaces a-Physicochemical and Engineering Aspects*, 2021, **612**.

37. V. Lopez, M. Rocio Villegas, V. Rodriguez, G. Villaverde, D. Lozano, A. Baeza and M. Vallet-Regi, Janus Mesoporous Silica Nanoparticles for Dual Targeting of Tumor Cells and Mitochondria, *ACS Appl. Mater. Interfaces*, 2017, **9**, 26697-26706.

38. L. G. B. Pereira, F. Petacci, J. B. Fernandes, A. G. Correa, P. C. Vieira, M. da Silva and O. Malaspina, Biological activity of astilbin from Dimorphandra mollis against Anticarsia gemmatalis and Spodoptera frugiperda, *Pest. Manage. Sci.*, 2002, **58**, 503-507.

39. D. R. Radu, C. Y. Lai, K. Jeftinija, E. W. Rowe, S. Jeftinija and V. S. Y. Lin, A polyamidoamine dendrimer-capped mesoporous silica nanosphere-based gene transfection reagent, *J. Am. Chem. Soc.*, 2004, **126**, 13216-13217.

40. R. Hikosaka, F. Nagata, M. Tomita and K. Kato, Adsorption and desorption characteristics of DNA onto the surface of amino functional mesoporous silica with various particle morphologies, *Colloids and Surfaces B-Biointerfaces*, 2016, **140**, 262-268.

41. A. E. Kaziem, Y. Gao, S. He and J. Li, Synthesis and Insecticidal Activity of Enzyme-

Triggered Functionalized Hollow Mesoporous Silica for Controlled Release, *J. Agric. Food. Chem.*, 2017, **65**, 7854-7864.

42. K. S. Walton and R. Q. Snurr, Applicability of the BET method for determining surface areas of microporous metal-organic frameworks, *J. Am. Chem. Soc.*, 2007, **129**, 8552-8556.

43. J. Choma, M. Jaroniec, W. Burakiewicz-Mortka and M. Kloske, Critical appraisal of classical methods for determination of mesopore size distributions of MCM-41 materials, *Appl. Surf. Sci.*, 2002, **196**, 216-223.

44. M. Yang, Y. Hao, J. Gao, Y. Zhang, W. Xu and L. Tao, Spinosad induces autophagy of Spodoptera frugiperda Sf9 cells and the activation of AMPK/mTOR signaling pathway, *Comparative Biochemistry and Physiology C-Toxicology & Pharmacology*, 2017, **195**, 52-59.

45. X. Lu, M. Hou, Q. Xia, C. Yan, Y. Xu and R. Liu, Mitochondrial targeted fluorescent probe with AIE characteristics for bioimaging, *Materials Science & Engineering C-Materials for Biological Applications*, 2017, **77**, 129-135.

46. M. Huang, A. K. S. Camara, D. F. Stowe, F. Qi and D. A. Beard, Mitochondrial inner membrane electrophysiology assessed by rhodamine-123 transport and fluorescence, *Ann Biomed Eng*, 2007, **35**, 1276-1285.

47. Y. Zhang, M. Luo, W. Xu, M. Yang, B. Wang, J. Gao, Y. Li and L. Tao, Avermectin Confers Its Cytotoxic Effects by Inducing DNA Damage and Mitochondria-Associated Apoptosis, *Journal of Agricultural & Food Chemistry*, 2016, **64**, 6895-6902.

48. S. Singh and M. Singh, Evaluation of Some Adjuvants for Improving Glyphosate

Efficacy, *Journal of Astm International*, 2005, **2**, 1-10.

49. F. Tang, L. Li and D. Chen, Mesoporous Silica Nanoparticles: Synthesis, Biocompatibility and Drug Delivery, *Adv. Mater.*, 2012, **24**, 1504-1534.

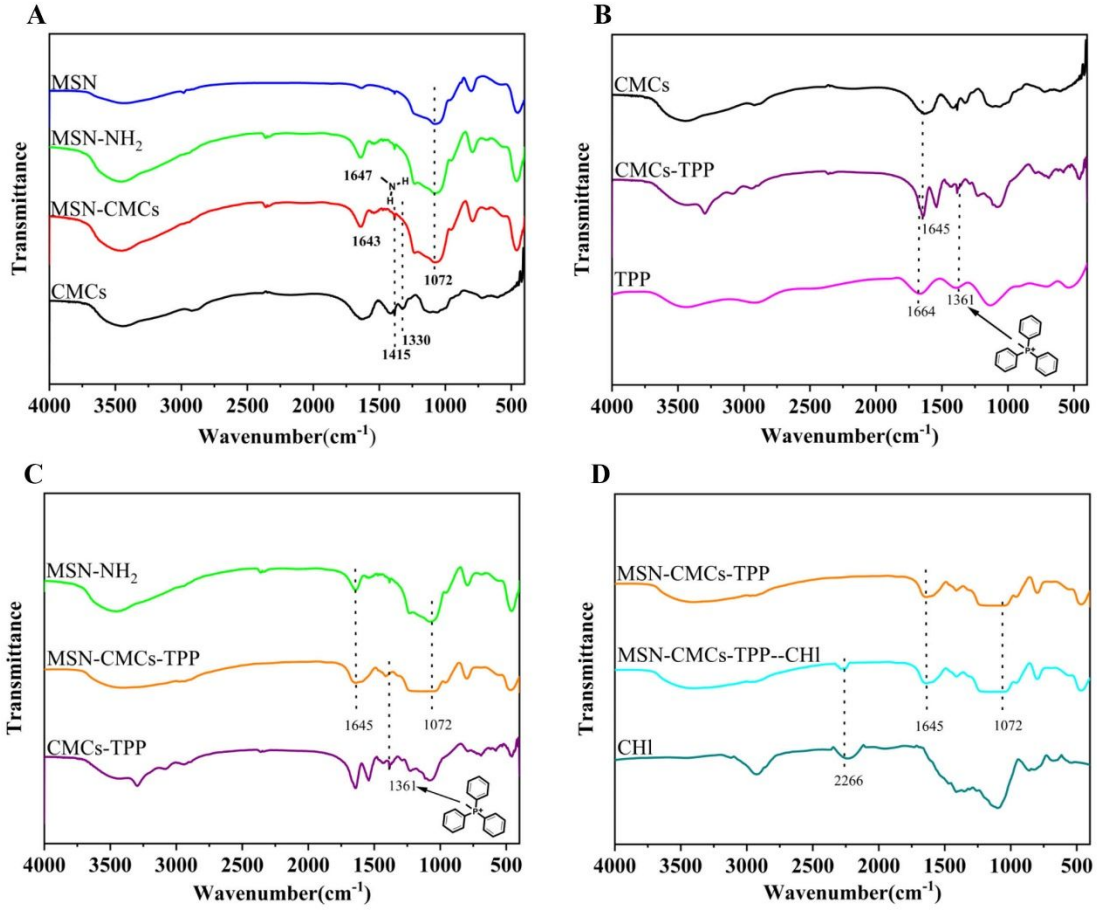

Figure 1. FT-IR spectra of nanoparticles. (A) MSN, MSN-NH_2, MSN-CMCs and CMCs; (B) CMCs, CMCs-TPP and TPP; (C) MSN-NH_2, MSN-CMCs-TPP and CMCs-TPP; (D) MSN-CMCs-TPP, MSN-CMCs-TPP-Chl and Chl.

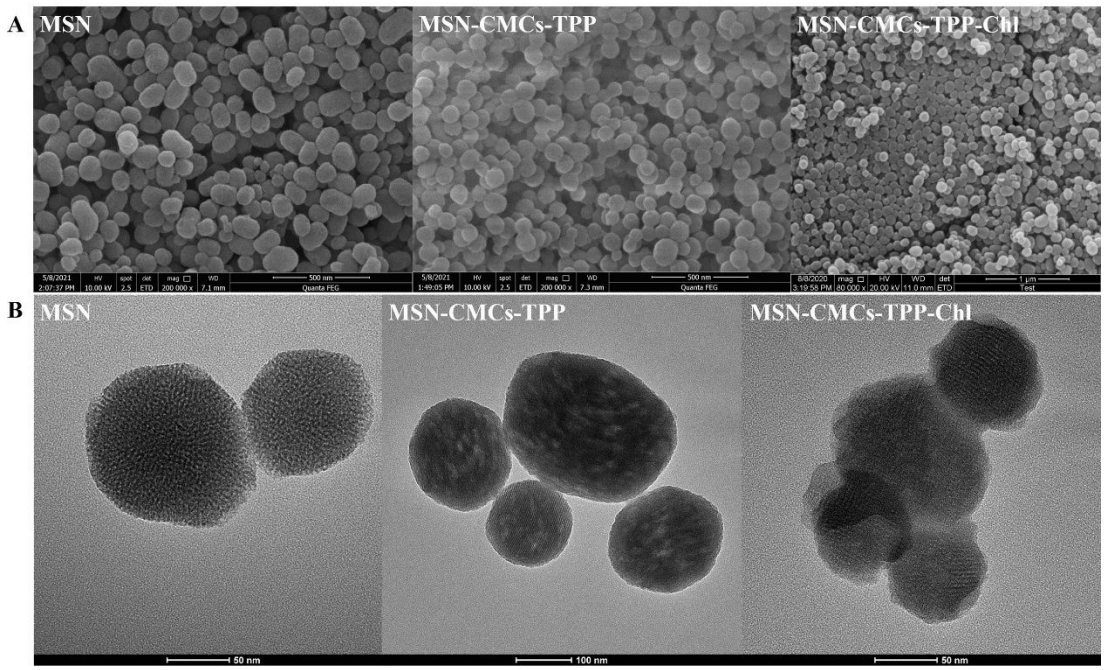

Figure 2. SEM and TEM images of nanoparticles. SEM: (A) MSN, MSN-CMCs-TPP, MSN-CMCs-TPP-Chl; TEM: (B) MSN, MSN-CMCs-TPP, MSN-CMCs-TPP-Chl.

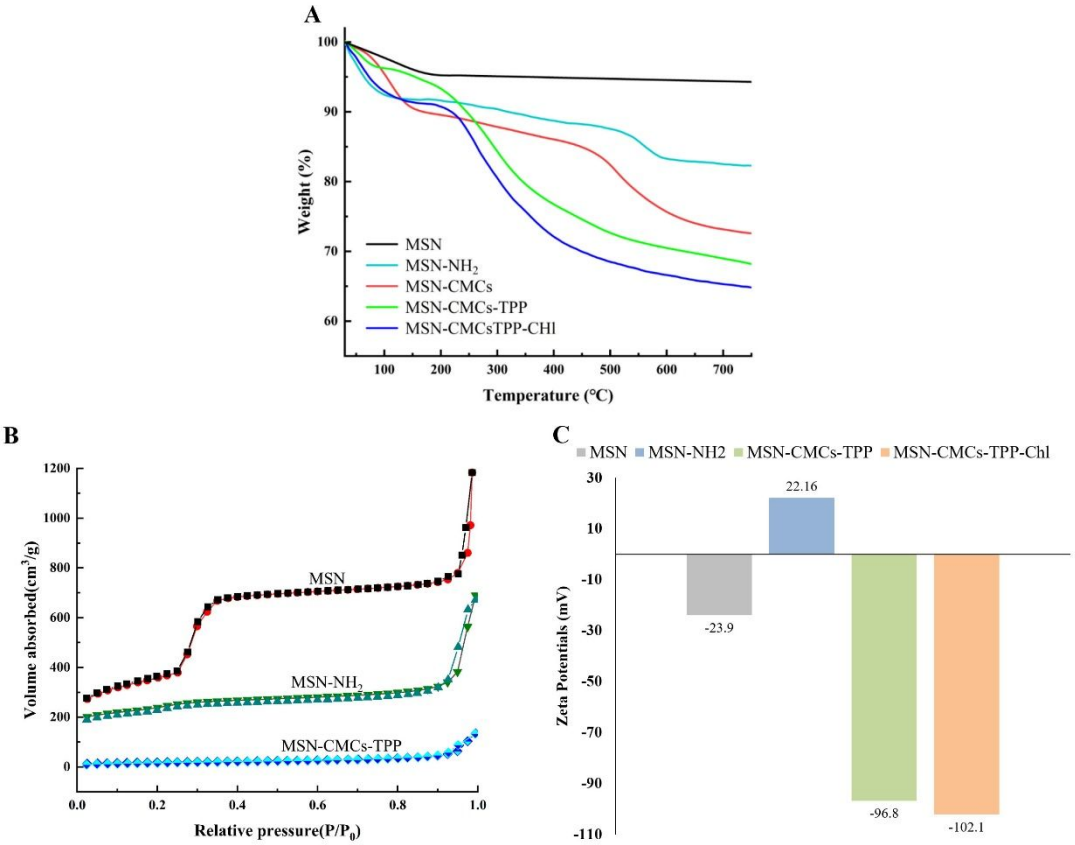

Figure 3. Characterization of the physicochemical properties of nanoparticles. TGA curves (A), Nitrogen adsorption-desorption isotherms (B) Zeta potentials (C) of nanoparticles.

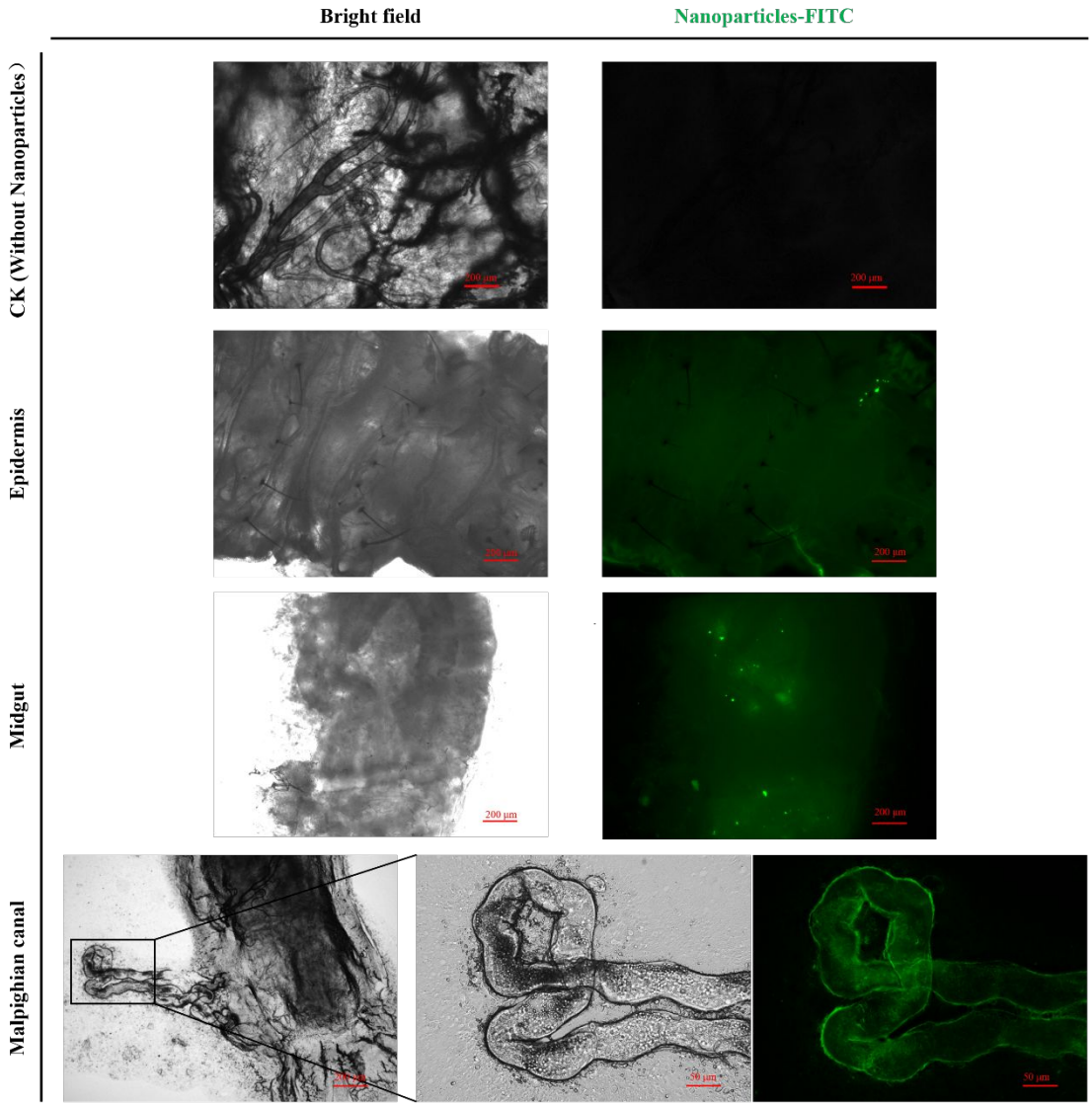

Figure 4. Fluorescence photomicrographs showing blank control (without nanocarrier) and treated group (the nanocarrier in the epidermis, midgut and Malpighian tubules). Larvae of *Spodoptera frugiperda* were treated with MSN-CMCs-TPP-FITC for 24 h. Representative fluorescence photomicrograph (×25, ×100) of epidermis, midgut and Malpighian tubules. The green fluorescence stands for nanoparticle carrier.

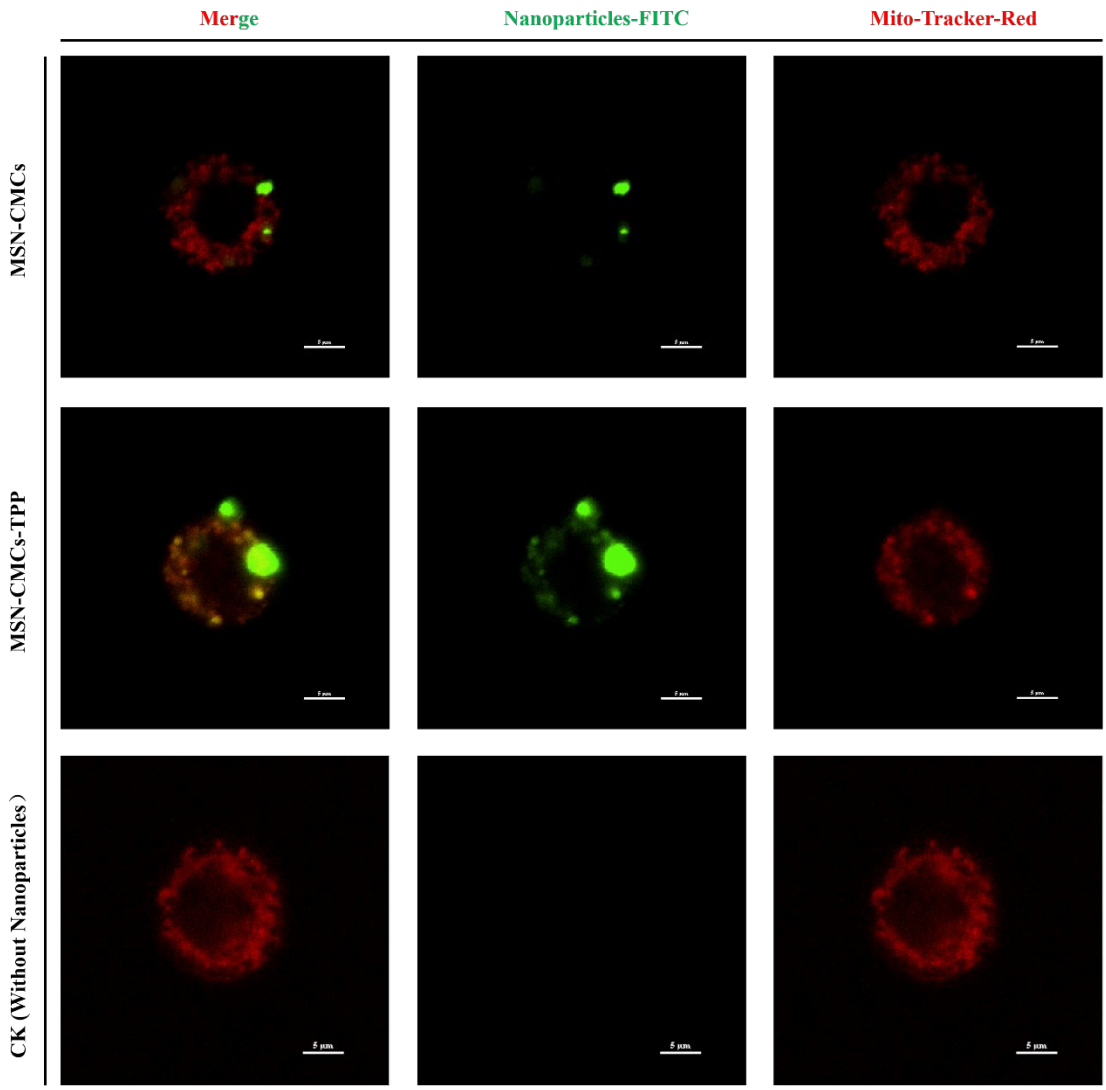

Figure 5. Confocal fluorescence photomicrographs showing Blank control, MSN-CMCs-FITC and MSN-CMCs-TPP-FITC on the mitochondria of Sf9 cells. Confocal fluorescence photomicrographs (×100) of Sf9 cells stained with Mito-Tracker Red and FITC. The red fluorescence stands for mitochondria and the green fluorescence stands for nanoparticle carrier.

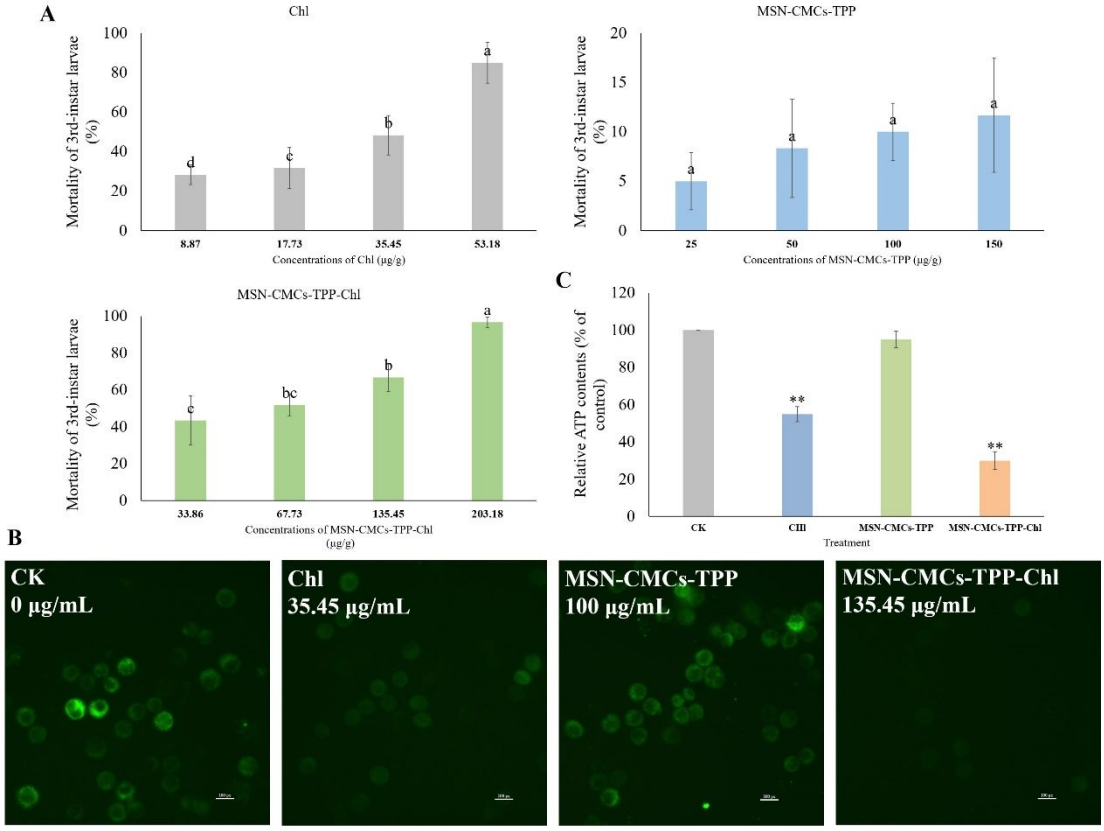

Figure 6. Enhancement of nanoparticle carriers on Chl toxicity. Toxicity of Chl, MSN-CMCs-TPP and MSN-CMCs-TPP-Chl on larvae of *Spodoptera frugiperda* (A); the loading content (%) of Chl is 35.45%, that is 135.45 g MSN-CMCs-TPP-Chl containing 100 g MSN-CMCs-TPP and 35.45 g Chl. Small alphabets indicate significant differences ($P \leq 0.05$) between any two groups. Fluorescence photomicrographs (×100) of Sf9 cells stained with Rh-123 after treatment with Chl (35.45 μg/mL), MSN-CMCs-TPP (100 μg/mL) and MSN-CMCs-TPP-Chl (135.45 μg/mL) (B). Relative ATP content was measured with commercial kits. Data are represented as the means ± SD by three independent replicates, $^{**}P \leq 0.01$ (C).

Table 1. Characterization of MSN and the modified MSNs

Sample	Size (nm)	S_{BET} (m^2/g)	V_t (cm^3/g)	Zeta (mV)
MSN	123	1358	1.23	-23.9
MSN-NH_2	130	678	0.36	22.16
MSN-CMCs-TPP	145	45	0.11	-96.80
MSN-CMCs-TPP-Chl	237	-	0.08	-102.10

Table 2. Comparison of loading efficiencies of Chl onto nanoparticle via different methods

Method	Sample	Loading content (%)	Encapsulation efficiency (%)
Impregnation method	MSN	40.15	86.40
	MSN-CMCs-TPP	2.30	4.20
emulsion synchronous encapsulation	MSN-CMCs-TPP	34.45	81.32

Table 3. Median lethal concentrations (LC50) of three treatments on the mortality of 3rd instar *spodoptera frugiperda*

	LC50 value by formulant (μg/mL)	LC50 value by Chl (μg/mL)	Toxicity regression equation (y=)	R^2
Chl	-	30.1	1.28x + 11.60	0.93
MSN-CMCs-TPP-CHl	62.7	16.4	0.31x + 30.71	0.97
MSN-CMCs-TPP	>150	-	0.05x + 4.80	0.90